Journal of Polymer Research (2018) 25: 217
https://doi.org/10.1007/s10965-018-1603-6

ORIGINAL PAPER

Microencapsulated self-healing polymers via controlled, surface initiated atom transfer radical polymerization from the surface of graphene oxide

Junali Handique[1] · Swapan Kumar Dolui[1]

Received: 31 March 2018 / Accepted: 20 August 2018 / Published online: 15 September 2018

Abstract

Polymers were grown directly on the surface of graphene oxide (GO). The method involved the covalent attachment of an atom transfer radical polymerization (ATRP) initiator on the surface of GO followed by the polymerization of methylmethacrylate, styrene or *t*-butyl acrylate using it as the macroinitiator. The surface initiated poly(methylmethacrylate) (PMMA-IGO) was embedded with microcapsules containing glycidyl methacrylate (GMA) to introduce self-healing property. The polymeric chains grown on the surface of the GO exhibited self-healing behaviour on rupture of the microcapsules. These polymer chains on the surface of GO preserved living characteristics and was able to resume copolymerization with released GMA on rupture of the microcapsules and get infiltrated into the cracks. As a result, the cracked planes were covalently re-bonded, offering almost 92% recovery of strength.

Keywords Surface initiated polymers · Atom transfer radical polymerization · Microencapsulation · Self-healing

Introduction

Spontaneous healing of injury is a key biomaterial feature and has lead the scientists and engineers to develop self-healing materials to improve the lifetime, safety, energy efficiency and environmental impact of man-made synthetic materials [1, 2]. Self-healing materials have the ability to regain their original strength after they are mechanically damaged, either internally or externally. Exhibiting such healing ability of the synthetic materials is a tedious job and it must contain some functionality, which will either react among themselves or couple with other functionality. Thus, smart selection of a controlled polymerization technique in combination with appropriate coupling reactions is highly recommendable. Encapsulation of monomers/crosslinker/catalyst into polymer matrix, supramolecular self-assembly, dynamic covalent bond formation etc. are the general adopted techniques for designing self-healing polymers [3–9]. Covalent bond formation, being the strongest chemical bonds, is undoubtedly the most efficient healing technique for long-term structural applications. A lot of methods are available for making self-healing polymers but only a few of them leads to formation of covalent bond between healing agent and the matrix [10, 11]. Microcapsule containing liquid healing agents for self-healing application is promising in terms of mass predictability and application popularity [12–14].

Surface initiated polymers (SIPs) have an advantage over other polymer architectures mainly due to their mechanical and chemical robustness, coupled with a high degree of synthetic flexibility towards the introduction of a variety of functional groups. Moreover they can be grown on a variety of functional surfaces and possesses the ability to resist hard operational conditions of solvent and temperature [15]. Although functionalization at the surface of graphene oxide may still be sterically limited, but still a large quantity of functional groups (either hydrophilic or hydrophobic) can be introduced through a surface initiated polymerization process, especially compared to macromolecular grafting-to approaches. Atom transfer radical polymerization (ATRP) is the most-utilized polymerization technique to synthesize self-healing SIPs as it provide excellent control over the molecular weight, polydispersity and composition of the polymers and are experimentally benign for further reactions [10, 16]. Furthermore, chain termination and chain transfer are absent in ATRP thus consisting of a living chain

✉ Swapan Kumar Dolui
swapankumardolui10@gmail.com

[1] Department of Chemical Sciences, Tezpur University, Napaam, Tezpur, Assam 784028, India

termini which can initiate further polymerization on availability of reactive monomer [2, 17]. SIPs can also be prepared by physisorption but it suffers from thermal and solvent instability, thus covalent attachment technique through ATRP is highly recommendable [18–25]. Hence, a system consisting of an encapsulated monomer pre-embedded in the living polymer chains of the matrix can repair the crack via covalent bond formation which can be termed as semi-encapsulation method. The mechanism involves the pre-embedded microcapsules containing healing agent are ruptured upon cracking and release the reparative substance into the cracked planes, which gets polymerized and rebond the damaged portions [26, 27]. Due to the infinitely long lives of the polymer chains, the encapsulated healing agent undergoes polymerization at ambient temperature wherever it meets the matrix as soon as the crack initiation or propagation starts. This copolymerization because of covalent bond formation through the healing process restores the original strength back to the SIPs. The covalently attached newly formed macromolecules attached to the interface, fill the interstitial space of cracks and fuse with the matrix. Development within this methodology offers significant potential towards increasing the service life of structural materials and decreasing maintenance costs.

Herein, we have synthesized surface initiated self-healing polymers from the surface of GO using ATRP and microencapsulation technique is applied to obtain the self-healability of the polymers with appropriate monomers. The efficiency of a microencapsulation self-healing technique can be further enhanced when functionality is increased on the matrix polymer. This gives an advantage for SIPs. Also GO is used as the surface material for growing polymers because it can undergo controlled, covalent functionalization and also facilitates improved physicochemical properties. ATRP initiator is first used to functionalize the hydroxyl groups present on the surface of GO and then polymers of MMA, styrene and *t*-BA were grown directly via a surface initiated polymerization. No extra initiator is required in this case wherein the GO functionalized initiator will itself act as the macroinitiator to carry out the polymerization. To confirm that the polymerization was indeed taking place from the surface of GO, a polymer cleavage experiment was carried out which confirmed the attachment of the polymer on the surface. Poly(melamine-formaldehyde) microcapsules containing GMA is used as the healing agent wherein the polymer chains attached to the surface of GO will attribute to self-healing ability. GMA was used as healing agent as it can be stored in room temperature for a considerable time and can also withstand high temperature processing condition without undergoing any polymerization. Moreover, it is a non-toxic low viscosity monomer and can undergo efficient copolymerization with living polymer matrix. To the best of our knowledge, self-healing SIPs from GO have not been studied in detail till now and this method offers a practical approach for the synthesis of self-healing materials based on GO by controlled, covalent functionalization of GO with synthetic polymers. Furthermore, the approach is versatile and facilitates access to GO derivatives that exhibit improved mechanical strength as well as dissolution properties along with self-healing property of the polymers.

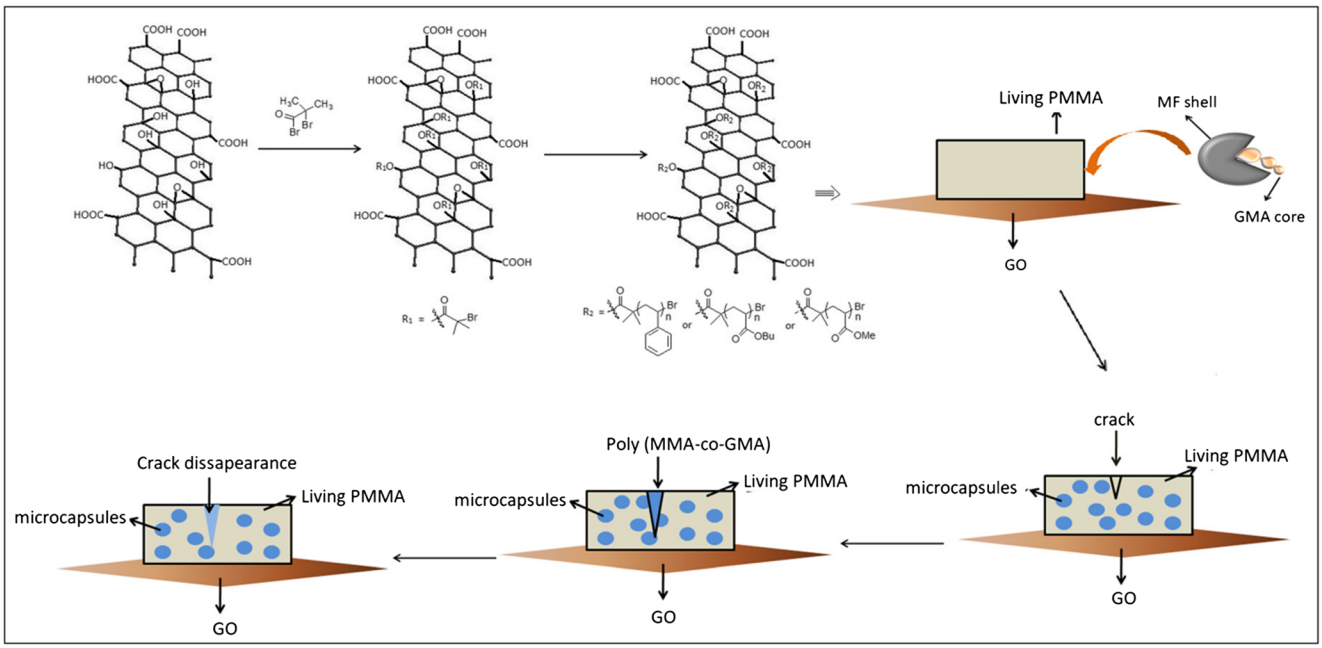

Scheme 1 The strategy for synthesis of self-healing SIPs by microencapsulation

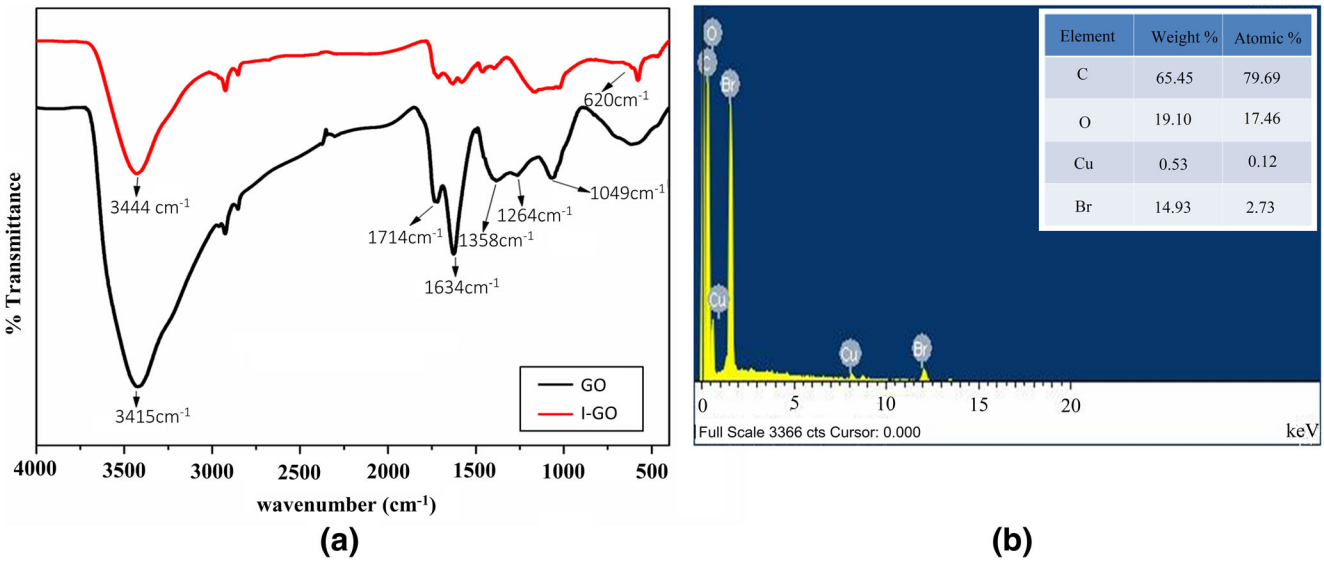

Fig. 1 FTIR spectra of GO and IGO (**a**) and EDX analysis of IGO (**b**) showing the presence of bromide functionality on the GO sheet

Experimental

Materials

Monomers Methylmethacrylate (MMA; Merck), Styrene (Merck), *t*-butyl acrylate (*t*-BA; Merck) were purified by washing with 5% Sodium Hydroxide (NaOH) followed by distilled water. α-bromoisobutyrylbromide (98%, Sigma), Triethylamine (TEA; Merck), Copper bromide (CuBr; 99.99%, Aldrich), N,N,N′,N″,N″-pentamethyldiethylenetriamine (PMDETA; 99%, Aldrich), Glycidylmethacrylate (GMA; 97%, Sigma-aldrich), Melamine (99%, Aldrich), Formaldehyde (37%, Aldrich), Sodium sulfate (Merck), Sodium bicarbonate ($NaHCO_3$; Merck), Sodiumdodecylbenzenesulfonate (SDBS; Aldrich), Poly(vinyl alcohol) (PVA; Aldrich, 87–90% hydrolyzed, average molecular weight 30,000–70,000), Methanol (99.8%, Merck) and 1-octanol (≥99%, Merck) were used as received. The solvents Dimethylsulfoxide (DMSO; 99.9%, Sigma-aldrich), Chloroform (99%, Merck), Dichloromethane (DCM) were dried using the standard methods prior to use.

Methods

Synthesis of graphene oxide based macroinitiator (I-GO)

I-GO was prepared by a simple esterification reaction of GO with α-bromoisobutyryl bromide. Graphene oxide (GO) was prepared from purified flake graphite using the traditional Hummers

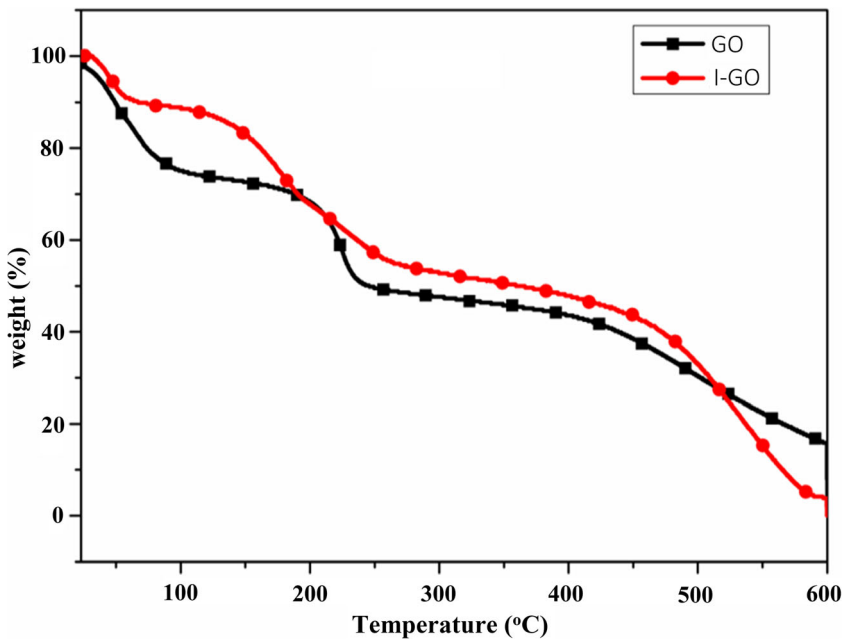

Fig. 2 TGA thermogram of GO and I-GO

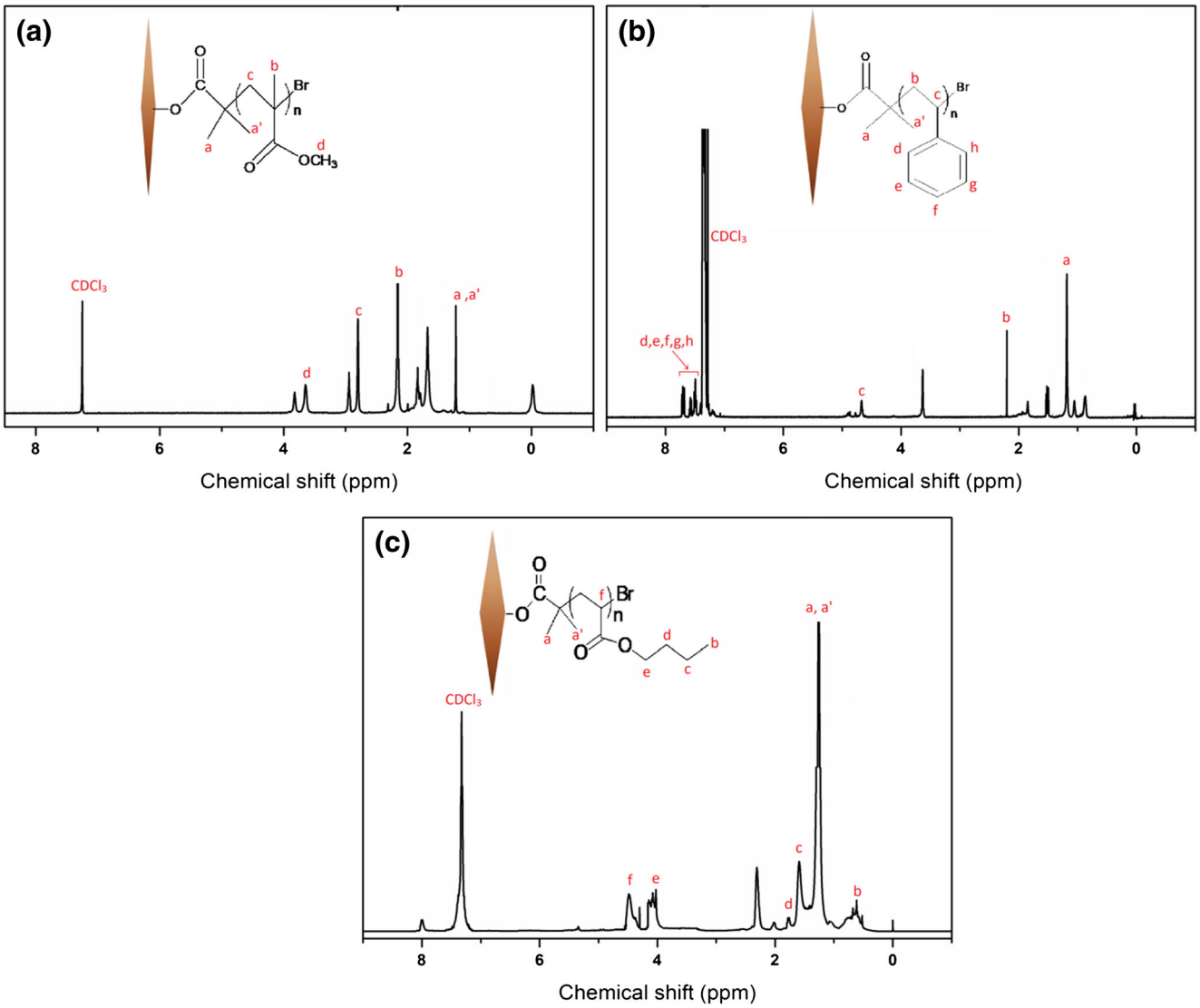

Fig. 3 ^{1}H NMR spectra of PMMA-IGO (**a**), PS-IGO (**b**) and PBA-IGO (**c**)

method [28]. A colloidal suspension of GO (1.00 g, 0.05 mg/mL in DMF) was prepared by sonication and the suspension was loaded into a round bottom flask. TEA (20 mL, 0.14 mol) was then added followed by addition of α-bromoisobutyrylbromide (30 mL, 0.2 mol) immersed in an ice-bath. The product was then filtered, washed with chloroform and deionized water and dried under high vacuum for 18 h.

Synthesis of SIPs using ATRP initiator I-GO (PMMA-IGO, PS-IGO and PBA-IGO)

ATRP using I-GO was carried out using three monomers MMA, styrene and *t*-BA. In a typical reaction 5 mL of the monomer was taken in a round-bottom flask equipped with a nitrogen inlet and magnetic stirrer and CuBr (0.036 g, 0.25 mmol), PMDETA (0.036 mL, 0.17 mmol) and DMF(5 mL) were added into it and stirred till light blue copper complex was formed. 0.1 g of I-GO was then added and stirred at 80 °C till a viscous solution was obtained. The resulting solution was then precipitated and washed with absolute alcohol (50 mL) followed by drying under high vacuum.

Cleavage of PMMA from the surface of GO (d-PMMA-IGO)

In a cleavage experiment, a solution of PMMA-IGO in DCM was taken in a 50 mL flask, followed by the addition of 2 mL of a saturated solution of $NaHCO_3$ in methanol. The mixture was stirred overnight at room temperature. The cleaved polymer was isolated by filtering through a Teflon membrane and thoroughly washing the residue with THF. The filtrate was then concentrated under vacuum, and the cleaved polymer was isolated by precipitation into methanol. After filtration, the product was dried under vacuum overnight.

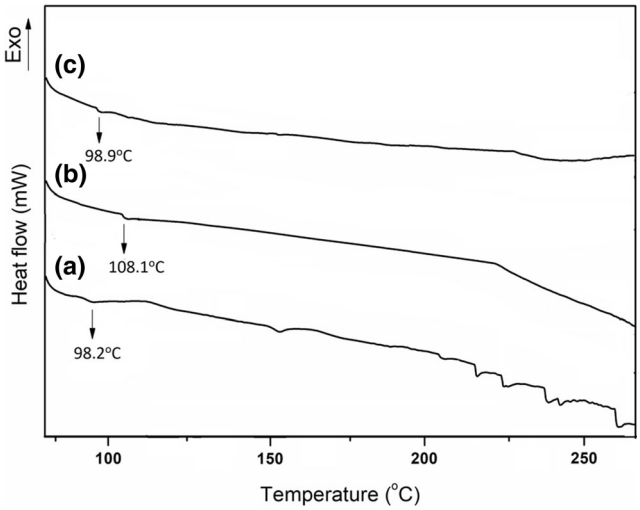

Fig. 4 DSC analysis of pristine PMMA (**a**), PMMA-IGO (**b**) and d-PMMA-IGO (**c**)

Synthesis of melamine-formaldehyde microcapsules containing GMA (MIC)

Melamine (12.2 g, 0.1 mol) and formaldehyde (37%, 5.69 g, 0.07 mol) were added to a 250 mL flask with deionized water and the pH was maintained to 8.5–9.0 under stirring at 70–80 °C. After prepolymer formation, SDBS, PVA solution and GMA were supplemented into it and pH was lowered to ~3.8. The reaction was carried out for 5 h. The speed of stirring affects the size of the microspheres. 1-octanol drops were added to remove resultant bubbles from stirring [29]. The microcapsule dispersion was cooled to room temperature, collected by filtration and washed with ethanol and distilled water followed by drying.

Table 1 Static water contact angle measurement of the SIPs

GO-Br surface	PMMA-IGO	PS-IGO	PBA-IGO
67°	71.9°	86°	84°

Synthesis of surface-initiated self-healing polymer

In a degassed three necked round bottom flask equipped with a vacuum line, nitrogen inlet, and magnetic stirring bar a mixture of MMA (5 mL, 0.05 mol), PMDETA (0.12 g, 0.7 mmol), CuBr (0.12 g, 0.8 mmol) were loaded. Soon after formation of blue copper complex, 0.1 g of I-GO was added and kept under stirring at 80 °C till free flowing viscous mass was formed. To the free flowing viscous mass, GMA loaded MF microcapsules were added under continuous nitrogen flow and allowed to mix well by stirring at a lower rate for about 5 min. The viscous mass was then transferred to a mold and kept under nitrogen atmosphere for about 48 h.

Characterization

FTIR spectra of the samples were recorded with a Nicolet Impact-410 IR spectrometer (USA) in KBr medium at room temperature in the range of 4000–400 cm^{-1}. NMR was measured by JEOL 400 MHz NMR instrument using $CDCl_3$ as solvent. Molecular weights and the polydispersity were measured by a gel permeation chromatography (GPC) instrument equipped with a Waters Styragel column (HR series 3, 4E) with THF as eluent at a flow rate of 0.7 mL/min. The surface morphology of the samples was determined by SEM (Jeol-JSM-6390LV) coupled with energy dispersive X-ray detector.

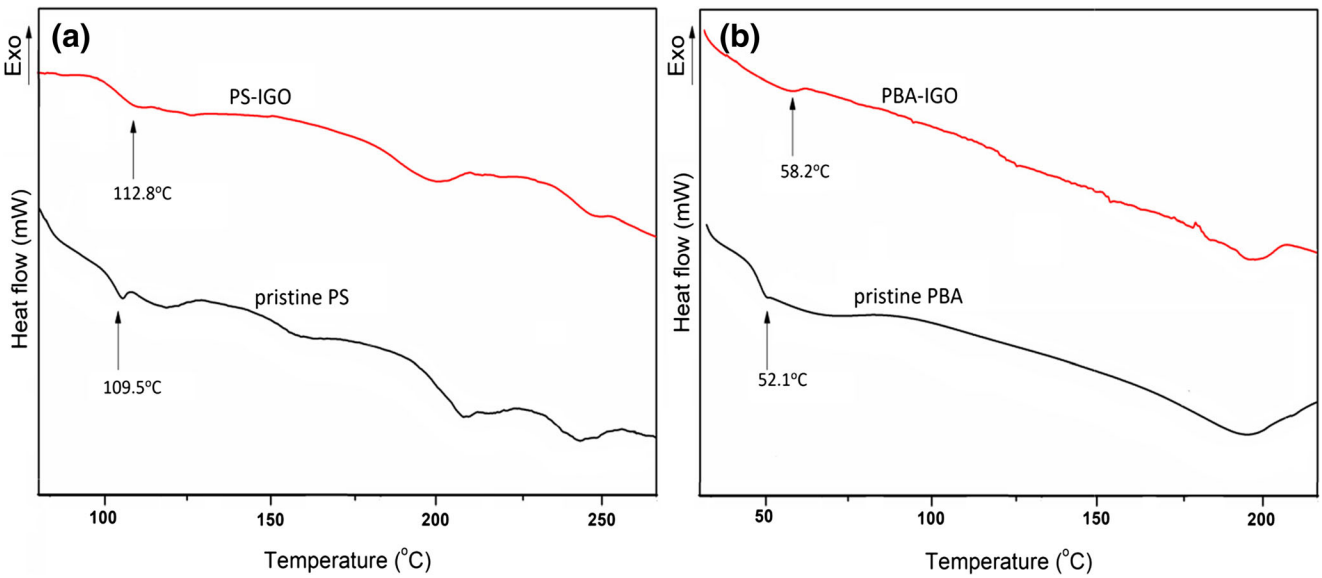

Fig. 5 DSC analysis of pristine PS and PS-IGO (**a**) and pristine PBA and PBA-IGO

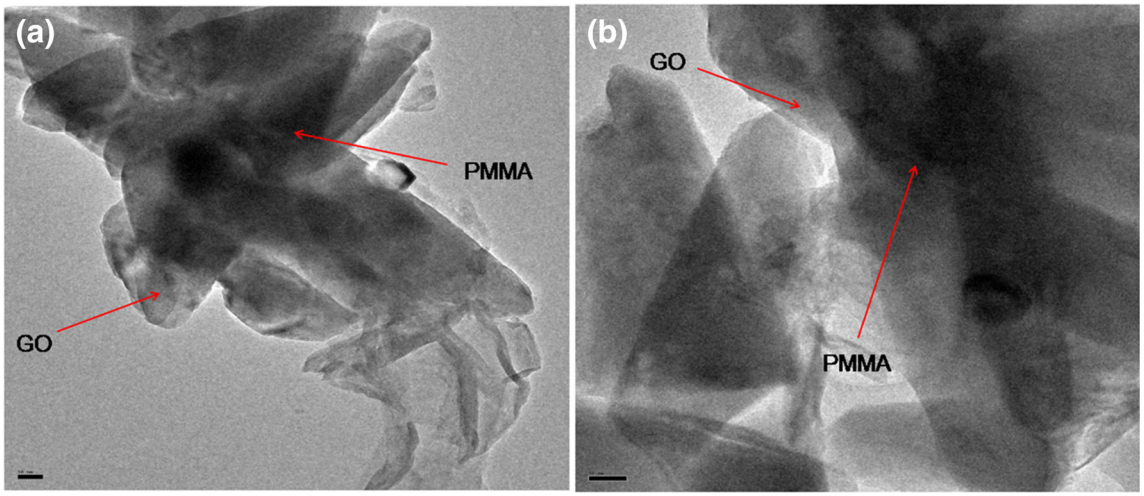

Fig. 6 **a and b** TEM images of surface initiated PMMA-IGO at two different positions (magnification: 50 nm)

Thermogravimetric analyses (TGA) was studied in a Shimadzu TA50 thermal analyzer under nitrogen atmosphere at a heating rate of 5 °C/min in the range of 30–600 °C. Differential Scanning Calorimetry (DSC) of the samples was conducted on a DSC-60, Shimadzu analyzer over a temperature range of 0° to 300 °C at a heating (or cooling) rate of 10 °C min^{-1} under a steady flow of ultrahigh-purity nitrogen purge. All the DSC curves were plotted from the second heating scan. The Hydrodynamic volume was measured using Nanotrac Wave Particle Size and Zeta Potential Analyzer and Eutech pH -700 was employed to measure the pH. TEM images were obtained from TECNAI G2 20 S-TWIN (200KV) using ethanol as the solvent. To evaluate self-healing ability of the materials, the method proposed by Jones et al. was employed to evaluate the self-healing ability of the polymers [30]. Healing efficiency, H_e is defined as:

$$H_e = \frac{\sigma_{healed}}{\sigma_{virgin}} \times 100\%$$

Tensile properties were examined using Universal Testing Machine (UTM, Zwick, Z010) at ambient temperature. Single edged notch bending test were conducted on the test specimens according to the ASTM standard D5045–99. Three samples were tested in each time. A loading rate of 10 mm/min was applied for the test. Razor blade prenotched samples were first broken to failure, giving the fracture toughness, σ_{virgin} and immediately clamped together and kept under nitrogen atmosphere to heal. Healed samples were tested again to measure the regained fracture toughness, $\sigma_{healed.}$ Condition.

Results and discussions

In this study, we have synthesized polymers from the surface of GO. We envisioned that the polymeric chains grown on the surface of the GO affords self-healing behaviour on rupture of the microcapsules. The synthetic strategy applied is described in Scheme 1. GO was first functionalized with ATRP initiator α-

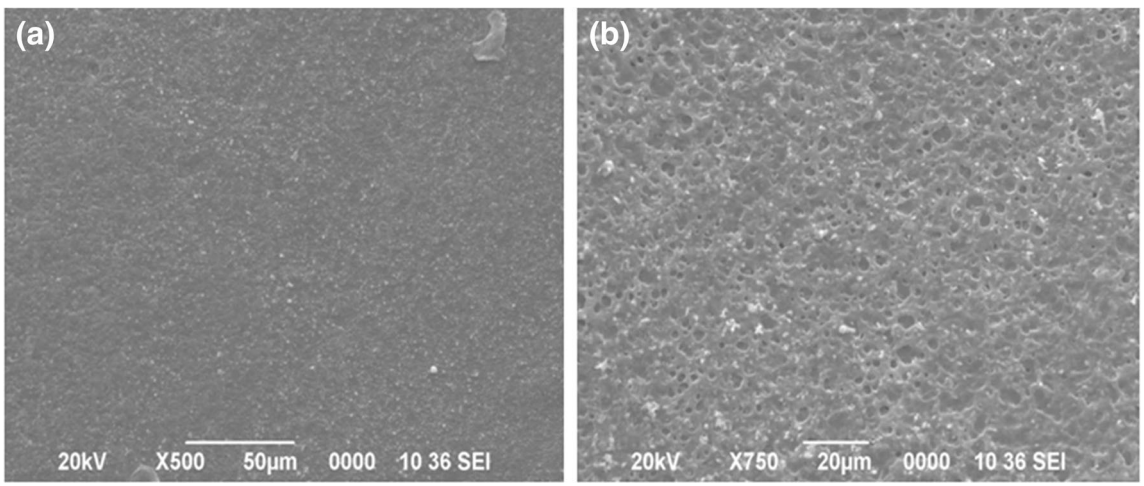

Fig. 7 SEM images of surface initiated PMMA-IGO at 50 µm magnification (**a**) and at 20 µm magnification (**b**)

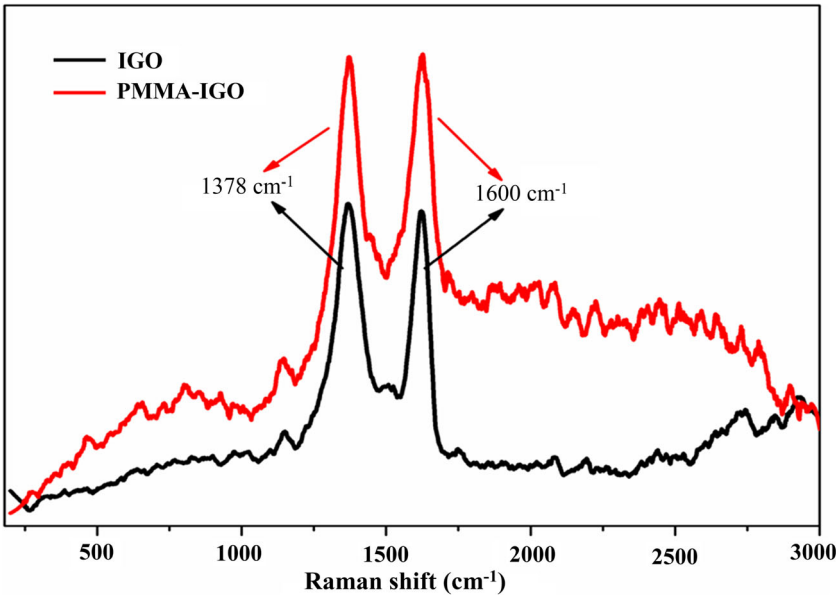

Fig. 8 Raman spectra of IGO and surface initiated PMMA-IGO

bromoisobutyrylbromide to get macroinitiator, I-GO. Polymethylmethacrylate (PMMA), Polystyrene (PS) and Poly(*t*-butylacrylate) (PBA) are then grown on the surface of GO by using I-GO as the macroinitiator and GMA loaded melamine-formaldehyde microcapsules (MIC) are embedded to initiate a self-healing reaction on rupture of the microcapsules.

Characterization of I-GO

The formation of I-GO was confirmed by FTIR (Fig. 1a). The pendant hydroxyl groups on the surface of GO was expected to undergo esterification with the acid bromide initiator in the formation of I-GO. In the spectrum of GO, all characteristic peaks can be observed at 3415 cm^{-1} (-OH stretching), 1714 cm^{-1} (-COOH), 1385 cm^{-1} (-OH deformation), 1634 cm^{-1}(unoxidized graphitic domains), 1231 cm^{-1}(-C-O epoxy) and 1061 cm^{-1} (-C-O alkoxy). After reacting GO with the aforementioned initiator, the same oxygen functional groups were still present, but signals attributed to the formation of C-Br bonds emerged at 750-500 cm^{-1} and the intensity of the signal attributed to -OH groups diminished at 3415 cm^{-1}.

EDX analysis in Fig. 1b revealed the presence of bromine providing further evidence that functionalization was successful in introducing the desired alkyl bromide functionalities onto the GO.

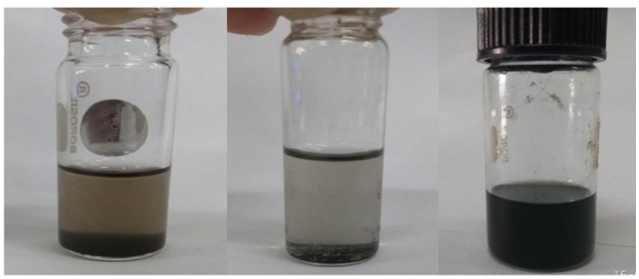

Fig. 9 Dispersion of GO after 7 h (**a**); as prepared IGO at 0 h (**b**); and PMMA-IGO after 7 h (**c**)

Figure 2 shows the TGA thermogram of the prepared I-GO to assess its thermal stability. GO is highly hydrophilic and store moisture in its p-stacked structure [31] therefore some mass loss was observed near 100 °C. Relatively a higher mass loss was observed around 170 °C due to oxygen-containing functionalionalities outgassing as oxides of carbon. The thermogram of I-GO shows a principal decomposition from 120 to 180 °C mainly because of the decomposition of the functional groups present in it. Notably, these decomposition pattern was not observed in the thermogram of unfunctionalized GO. After the decomposition of the thermally labile oxygen and initiator groups in I-GO, no considerable mass loss was observed upto 490 °C, after which degradation of the carbon framework occurs.

Characterization of SIPs

After the successful synthesis and characterization of I-GO, the synthesis of SIPs in a controlled fashion was demonstrated. The ^{1}H NMR spectra (Fig. 3) of the polymers verified that the polymerizations from the functionalized GO surface was successfully conducted. The characteristic peaks of PMMA grown from surface of GO were observed at $\delta = 3.5, 2.2$ and 1.0 ppm for $-OCH_3$, $-CH_2$ and $-CH_3$ respectively (Fig. 3a). Similarly the characteristic peaks for PS and PBA were also observed (Fig. 3b and c).

Another parameter to observe the synthesis of SIPs is the glass transition temperature (T_g). The T_g increased from 98.2 °C in pristine PMMA (Fig. 4) to 108.1 °C for PMMA-IGO. Moreover the DSC curve of d-PMMA-IGO also shows the T_g again decreased to about 98.9 °C which clearly indicates the detachment of PMMA polymer chains from the surface of GO. Similarly the T_g for PS-IGO and PBA-IGO

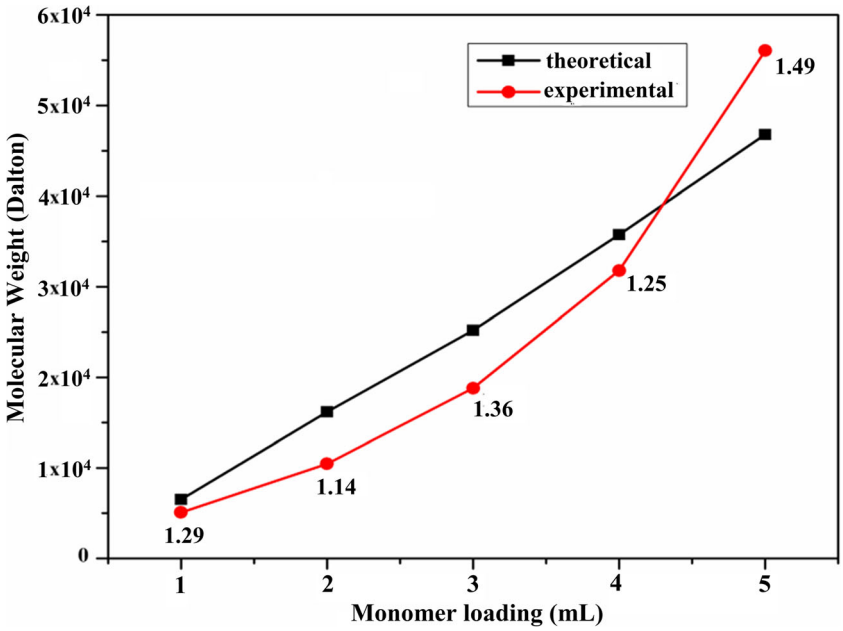

Fig. 10 Variation of molecular weights of d-PMMA-IGO-1-5 with increase in MMA loading

(Fig. 5) also increased from its corresponding bulk counterpart. It has previously been reported that attachment of polymer chains to silica nanoparticle surfaces leads to chains constraint which results in increase of T_g [32, 33]. The same phenomenon may be occurring in this case also, where the attachment of polymer chains to GO imposes restraint over their mobility, resulting in the observed 4–10 °C increase in T_g. This indicates that the elevated T_g is the result of the attachment of the polymers to the surface of GO.

The average static water contact angles of PMMA-IGO, PS-IGO and PBA-IGO surfaces in Table 1 increased to about 71.9° for PMMA-IGO, 69° for PS-IGO and 84° for PBA-IGO from about 67° for original GO-Br surface [34]. This results indicates that aforementioned polymers has been successfully grafted on the GO-Br surface.

TEM and SEM images of PMMA-IGO

The structure of PMMA-IGO was examined by TEM shown in Fig. 6a and b. The image shows layer of GO sheet attached with tufts of polymer protuberances evenly dispersed on the whole sheet [35] along with fine coating covering the black surface of GO uniformly. The darker portions represented the surface of GO; the portions outside was that of PMMA. Therefore, it is reasonable to conclude that PMMA is grafted onto the GO surface.

From the SEM images in Fig. 7, it appears that the functionalized platelets became wrinkled during the sample preparation. However, it is clear that the polymer chains covered the convoluted surfaces of the platelets. Therefore, it is reasonable to conclude that the PMMA is grafted onto the GO surface. Also, SEM images showed significant changes in surface morphology and roughness, demonstrating the presence of PMMA.

Raman spectra of I-GO and PMMA-IGO

The Raman spectra of I-GO and PMMA-IGO shows the characteristic tangential mode signals (G band) and disorder mode signals (D band) at $\nu = 1600$ and 1378 cm^{-1}, respectively in Fig. 8. Subsequently the D/G ratio for I-GO and PMMA-IGO was found to be constant at 1.2. The D/G ratio for GO was also

Table 2 Various conditions for synthesis of MIC

Feeding wt. ratio of core/shell raw materials	SDBS (wt%)	PVA (*W/V*)	Agitation rate (rpm)	Average diameter (μm)	Core content (%)
2	1.0	0.3	400	189.4 ± 7.5	87.7 ± 8.4
2	1.0	0.3	500	90.2 ± 8.8	71.1 ± 6.2
2	2.0	0.3	300	212.6 ± 5.8	78.8.2 ± 2.5
2	2.0	0.3	500	70.8 ± 9.6	85.6 ± 6.9
2	2.0	0.3	700	42.6 ± 7.9	55.8 ± 5.5

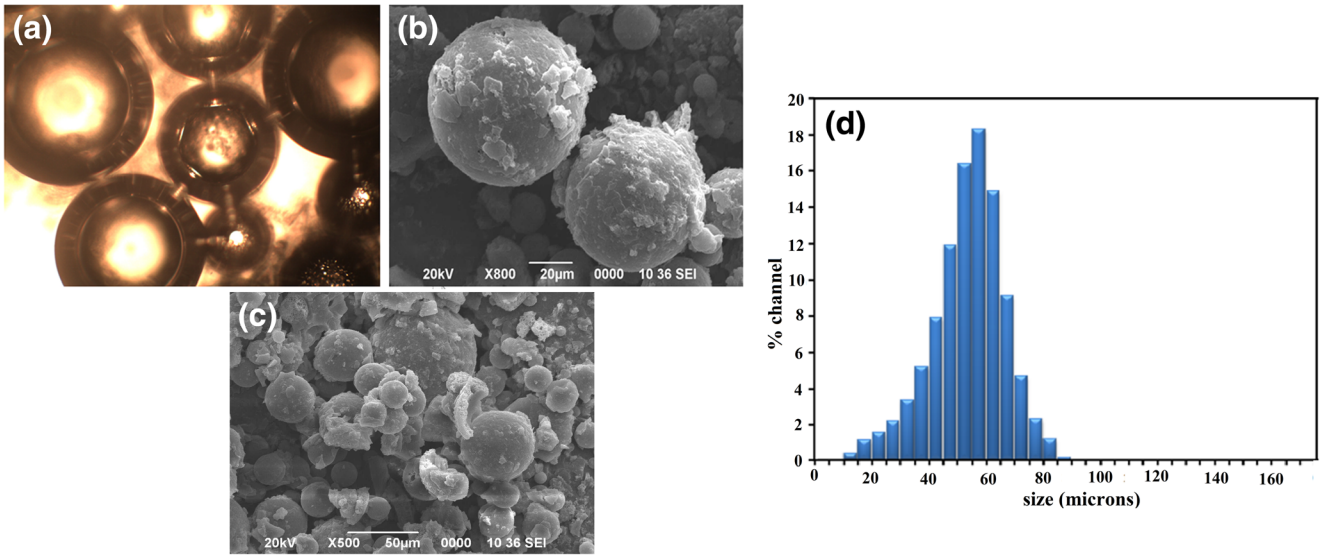

Fig. 11 Optical microscopy image of the MF-microcapsules containing GMA (**a**), SEM image of the microcapsules showing deposited nanocapsules (**b**, **c**) and Size distribution histogram of the MF-microcapules containing GMA (**d**)

reported to be 1.2 which clearly indicates that both IGO and PMMA-IGO maintains its characteristic mode signals for GO even after functionalization [34].

Dispersion study of GO, I-GO and PMMA-IGO in THF

In addition, the dispersion experiment was carried out to evaluate the functionalization effect. The photographs for GO, I-GO and PMMA-IGO after dispersion in THF are illustrated in Fig. 9. GO on dispersion in THF displays relatively short-term stability and precipitated completely in a matter of days. This result coincides with results obtained by Paredes et al. [36]. In case of I-GO, no compatibility is observed with the solvent and it settled down. This is because of the presence of few additional carbonyl and carboxyl groups located at the edge of I-GO, which is incompatible with most organic solvents and also the hydroxyl groups present are mostly functionalized with the initiator. The PMMA-IGO however shows compatiblility with solvents, rendering them dispersible in THF and stable for almost 4–5 days.

GPC measurements

In order to further confirm that the polymerization of MMA is indeed taking place from the surface of GO, we varied the amount of MMA loading (1 mL, 2 mL, 3 mL, 4 mL, 5 mL)

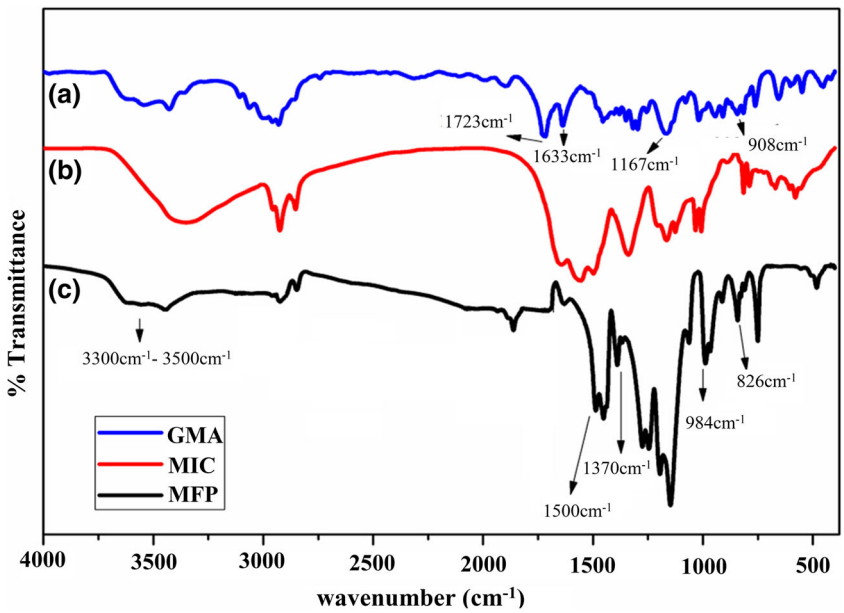

Fig. 12 FTIR spectra of GMA (**a**), MIC (**b**) MFP (**c**)

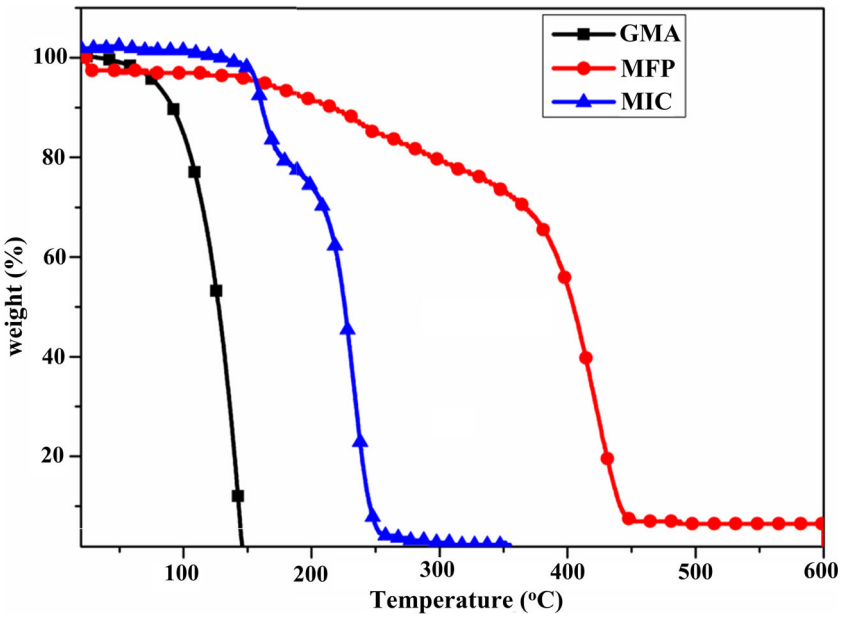

Fig. 13 TGA thermogram of GMA, MFP and MIC

relative to a fixed amount of IGO. The PMMA-IGO chains were then detached from the surface of GO via saponification with $NaHCO_3$ in a mixture of MeOH–CH_2Cl_2 (2:7 *v*/v) [37] to get d-PMMA-IGO. As shown in Fig. 10, the molecular weights of d-PMMA-IGO as given by GPC increased in accordance with the amount of monomer loaded (i.e. d-PMMA-IGO-1-5 were detached from PMMA-IGO-1–5, respectively). Additionally, the d-PMMA-IGO-1-5 exhibited relatively low PDI implying that the polymerization proceeded in a controlled manner, despite of being initiated from the surface of GO. From the elemental analysis, the theoretical molecular weight calculated based on the initial initiator concentration with respect to GO were in good agreement with their experimentally determined values.

Microcapsules characterization

In order to study the self-healing property of PMMA-IGO, microcapsules containing GMA under different conditions were synthesized via in-situ condensation method and is given in Table 2. The data indicates that both core content and diameter of the microcapsules is greatly influenced by the agitation rate. An increase in the agitation rate leads to breaking of oil droplets which favours the formation of finer emulsion,

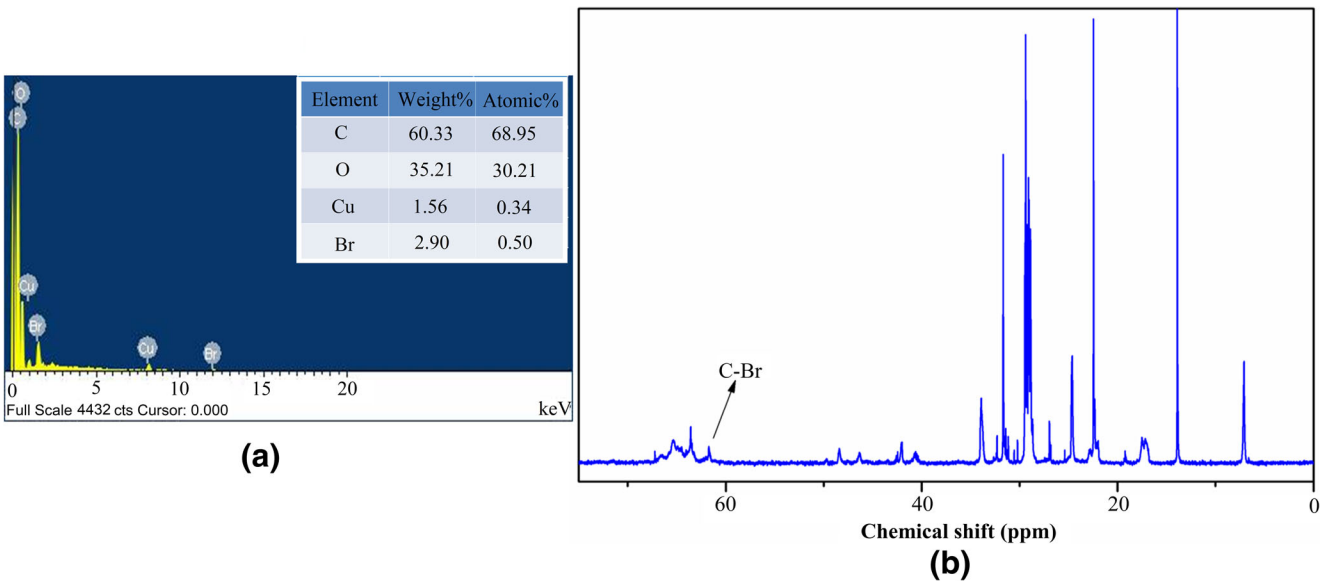

Fig. 14 EDX analysis of PMMA-IGO showing the presence of bromide group (a) and ^{13}C NMR spectra of PMMA-IGO showing the presence of bromide group

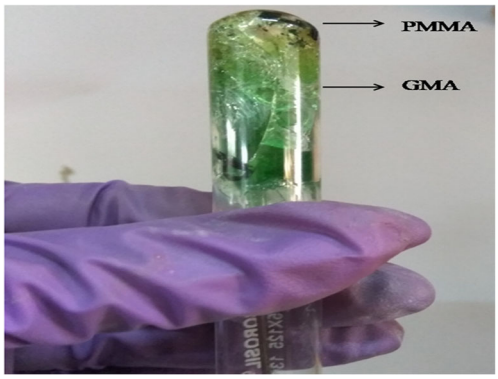

Fig. 15 A typical run of experiment showing the precipitation of d-PMMA and GMA copolymer in ethanol

and forms microcapsules with smaller size and narrower size distribution [38]. As a result, stirring speed is inversely proportional to both size and size distribution of the microcapsules formed. Accordingly, the relative quantity of the core material i.e. core content is also reduced with a rise in the agitation rate. This coincides with the results attained by other researchers [9, 38, 39]. The core content of the microcapsule was determined by extraction method. The process includes the crushing of the microcapsules and then extracted via Soxhlet apparatus for 72 h using acetone as an extraction solvent to remove the core material.

The % core content, W_{core} was thus calculated by using the formula:

$$W_{core} = \frac{W_1 - W_2}{W_1} \times 100\%$$

where, W_1 and W_2 denote the mass of microcapsules before and after extraction, respectively.

The formation of microcapsules was initially examined by optical microscopy shown in Fig.11a. It clearly indicates the formation of spherical microcapsules of similar size. The appearance of diffraction rings indicates that the healing agent is successfully incorporated inside the microcapsules. From the SEM images (Fig. 11b, c), it can be observed that the microcapsules are spherical and the surfaces are smooth with some deposited nanocapsules. The better adhesion of the microcapsules are further enhanced by the presence of these protruding MF nanoparticles.

Furthermore, the size distribution histogram of the microcapsules determined by DLS also shows the size of the microcapsules to be varying between 60 and 80 μm as shown in the Fig. 11d. This size is ideal to carry out a self-healing reaction. Size of the microcapsule was found to be distributed within a wide range but the size of major part of the microcapsules varies between 60 and 80 μm. The reason may be due to the

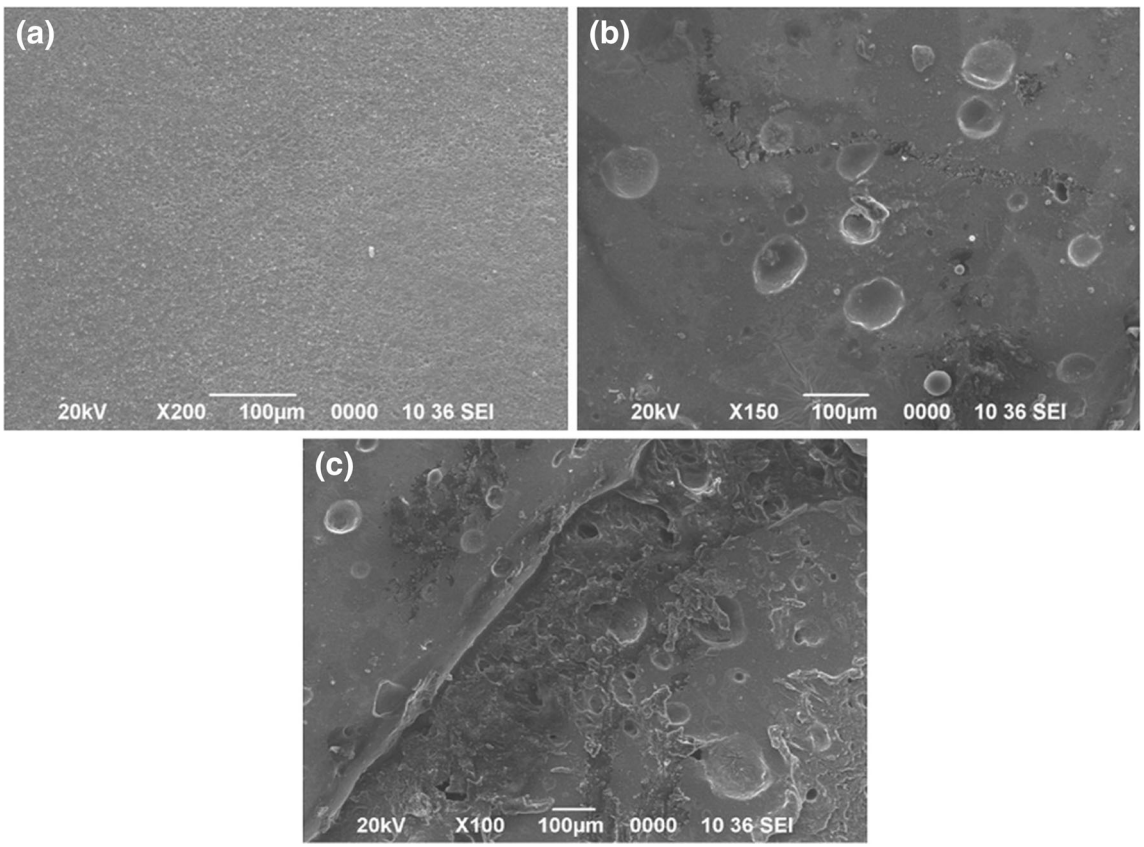

Fig. 16 SEM images of the surface of the polymer without microcapsules (**a**) and containing microcapsules (**b**) and fracture surface of PMMA-IGO sample containing microcapsules (**c**)

Table 3 Results of control tests with unfilled Surface initiated living PMMA

Healing agent	Healing condition	Strength of healed specimens(MPa)	Healing efficiency(%)
Hydroquinone(0.1 wt%) dissolved GMA	rt, 50 h, N_2 atm.	0.887 ± 0.043	28.2 ± 0.6
Injected GMA	rt, 50 h, N_2 atm.	3.41 ± 0.08	87.2 ± 1.21
No GMA	rt, 50 h, N_2 atm.	0	0

fact that the fluid flow around the propeller is turbulent, in the region of flow away from the propeller, many larger microeddies exist, and in the vicinity of the propeller blades, many smaller microeddies exist, resulting a wider capsule size distribution [40].

Figure 12 shows the FTIR spectra of the GMA, MIC and MFP shell wall. The spectrum of GMA(a) shows all the characteristic peaks for -C=O stretching mode at 1723 cm^{-1}, -C-O-C at 1167 cm^{-1}, -C=C stretching mode at 1633 cm^{-1} and epoxy group at 908 cm^{-1} respectively. The MFP spectrum (c) exhibits a board stretching vibration of -NH and -OH at 3300–3500 cm^{-1}, -CN stretching at 1500 cm^{-1}, C-H bending at 1310 cm^{-1}, -CO-NH stretching at 992 cm^{-1} and triazine ring stretching at 826 cm^{-1}. The spectrum of the MIC(b) shows all the characteristic peaks of both GMA and MFP indicating that GMA must have been encapsulated by MFP as expected.

Figure 13 shows the TGA thermogram of GMA, MFP and MIC. The decomposition of MIC consists of two stages. In the first stage of 100–200 °C, high temperature accelerates the diffusion of GMA absorbed on the MFP shell wall because of its high volatile nature, and an appreciable weight loss appears. As there is continuous rising of temperature, the encapsulated GMA inside the microcapsules gasifies thus causing a sharp decline of residue weight at 252.51 °C. But as compared with raw GMA which is a highly volatile compound, the thermal stability of the encapsulated GMA inside the microcapsules is evidently increased owing to the shielding of the MFP shell wall as MFP clearly has very high thermal stability. These facts clearly indicates that the thermal stability of GMA core with the MFP shell is higher as compared to the unshielded raw GMA. Additionally, the residue weight of MFP shell wall at 600 °C has a residue weight of 8.08 wt.%, as compared to MIC which has a residue weight of only 1.48 wt.% at the same temperature, which further evidences that MIC have higher core content.

Self-healing study

The main aim of the aforementioned study is to develop a self-healing polymer by microencapsulation technique using ATRP. A common feature of polymers prepared by ATRP is that they carry a bromide group at one end of the chain and thus the living PMMA chains can further undergo co-polymerization with GMA to mend the cracks. To confirm that PMMA-IGO indeed consist of a bromide group in its chain, EDX analysis was carried out which confirmed its presence as shown in Fig. 14a.

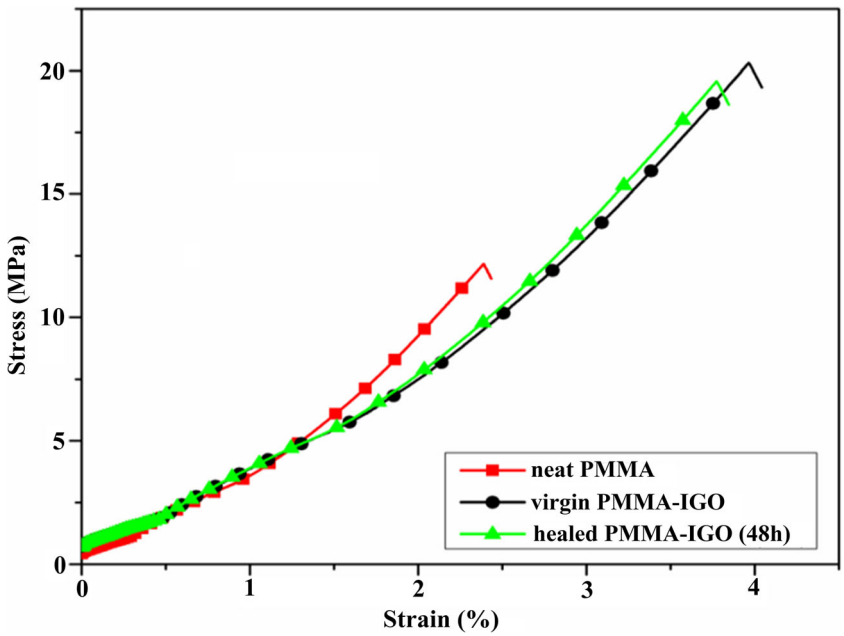

Fig. 17 Stress-strain curve of neat PMMA, surface initiated PMMA (PMMA-IGO) and surface initiated PMMA after healing (PMMA-IGO, 48 h) (3 samples are tested in each case)

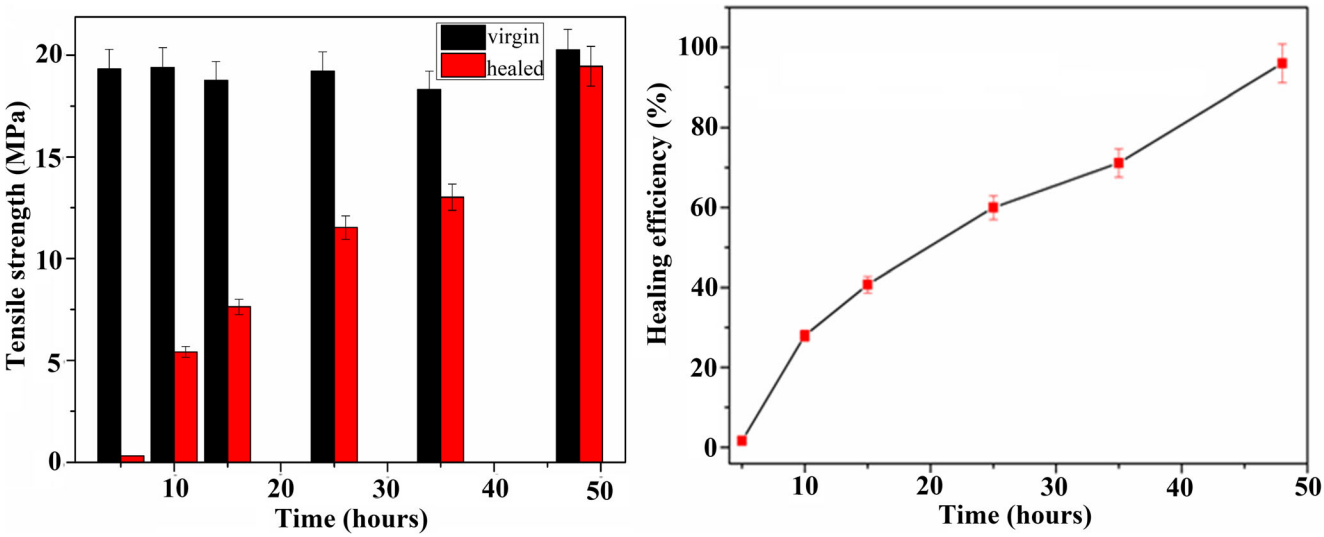

Fig. 18 Tensile strength of PMMA-IGO before and after healing (**a**) and Healing efficiency of the PMMA-IGO with added microcapsules (**b**)

In fact, the living characteristics of PMMA-IGO can also be examined in an intuitive way as follows. First, bulk PMMA was detached from GO by saponification method using $NaHCO_3$ in DMF. The ^{13}C NMR spectra of the detached polymer d-PMMA-IGO confirm the presence of bromide group at the end of the chain as shown in Fig. 14b. The peak at $\delta = 62$ ppm for PMMA is attributed to the presence of C-Br group present in its chain.

The d-PMMA-IGO so obtained was then taken in a test tube and GMA was added into it. If the d-PMMA-IGO possesses initiating activity as other living polymers, it will form a copolymer with GMA. As seen in Fig. 15, a two layered solid mass is obtained which confirms that the d-PMMA-IGO retains the living characteristics. Whenever the monomer encapsulated inside the microcapsules meets the matrix, it will undergo polymerization and hence heal the cracks. The unclear interfaces in between the layers indicate the diffusion of monomers and formation of copolymer. On the whole, the results indicates that the surface of living PMMA-IGO is able to resume polymerization as long as the monomers are available. In other words, when the liquid healing agent (i.e. GMA monomer) coming out from the broken microcapsules meets the PMMA chains of PMMA-IGO matrix, it would get copolymerized so that the cracks can be healed.

Self-healing performance

As mentioned in the experimental section, the self-healing PMMA-IGO sample was fabricated by loading in-situ GMA containing MFP microcapsules onto the living polymer matrix. SEM images of the surface of the polymer containing microcapsules and without microcapsules are shown in Fig. 16a, b. This indicates that the incorporated microcapsules are well adhered inside the matrix and retains their integrity without undergoing any damage during processing conditions.

Figure 16c further shows the fracture surfaces of healed PMMA-IGO composites. It is seen that the GMA healing agent cover the fracture surfaces after being liberated from the cloven microcapsules and converted into solidified membrane. It coincides with the evidences of living characteristics of the PMMA-IGO matrix discussed in the last sub-section. Such a product resulting from the copolymerization of GMA and living PMMA-IGO matrix must be able to reconnect the cracks in PMMA chains. The data in Fig. 18b give support to this deduction. The healing efficiency increases with increasing time, attains 50% after 23 h, and reaches the maximum healing of 92% after 48 h. Accordingly, a conservative healing period of 48 h should be appropriate for healing at room temperature. Clearly, the proposed concept of making self healing polymer based on ATRP works.

Table 4 Healing efficiency and fracture toughness of PMMA-IGO containing microcapsules

Microcapsules content (wt.%)	Average fracture toughness of virgin specimens (MPa)	Fracture toughness of healed specimens (MPa)	Healing efficiency(%)
0	12.5 ± 2.5	0	0
2.5	10.2 ± 4.3	6.4 ± 5.3	62.7
5	9.6 ± 7.8	6.7 ± 2.4	69.7
10	7.4 ± 5.8	6.0 ± 47	81.08
15	6.2 ± 2.8	5.7 ± 7.8	91.9

It is worth noting that GMA being a small molecule-solvent, so the crack healing behaviour might originate from swollen driven entanglement of PMMA chains across the cracked planes. Hence, a controlled experiment was performed to determine the solvent effect on healing efficiency and the results are shown in Table 3. Accordingly, a hydroquinone dissolved GMA was manually injected onto fracture surface of the living PMMA-IGO control specimens in which no GMA-loaded microcapsules were incorporated, and then the specimen was healed at room temperature under nitrogen atmosphere. Because p-hydroquinone being an inhibitor of the polymerization, the possible copolymerization reaction between GMA and living PMMA chains of PMMA-IGO could not proceed. If healing would have taken place in this case, the solvent effect of GMA must have come into action. Mechanical tests experiments comes in favour of this and shows that the pure solvent effect of GMA on healing ability leads to only about 28% healing efficiency. On the other hand, to give an idea of the maximum healing performance of the present system, pure GMA monomer was injected onto PMMA-IGO specimen without GMA-loaded microcapsules under nitrogen atmosphere. Afterwards, the damaged specimens were healed at room temperature for 50 h and the healing efficiency was found to be 87%. Comparison of the results of these two control experiments, it can be concluded that living polymerization induced chemical bonding rather than solvent effect is the main contributor to the crack repair. Furthermore, the data in Table 3 manifest that neat surface initiated PMMA has no healing ability under the present healing conditions when no healing agent is supplied.

The stress-strain curve for virgin PMMA and also for PMMA-IGO before and after healing are shown in Fig. 17. It is observed that the strength of PMMA-IGO as expected increases in comparison to that of virgin PMMA which confirms the attachment of PMMA onto its surface [41]. Accordingly the stress-strain of the healed PMMA-IGO film after 48 h of healing also shows almost 92% retention of its strength.

The tensile strength of PMMA-IGO samples before and after healing along with its healing efficiency are shown in Fig. 18. The healing efficiency of the polymer shows an exponential increase with time. This is because of the fact that with increasing time more and more healant flows to the cracked plane. The healing efficiency reached 92% after 48 h.

The influence of microcapsules concentration is very important and should be understood as the ultimate healing efficiency is a function of the amount of the released healing agent [42]. As illustrated in Table 4, healing efficiency of the polymer matrix remarkably increases with increase in capsules content thus following the general law of extrinsic self-healing composites containing microencapsulated healing agent. However, fracture toughness of PMMA-IGO decreases with increasing the amount of microcapsules. Such a reduction in toughness of brittle matrix due to addition of healing capsules is consistent with the results of a linear PS matrix containing microcapsules [40]. Considering that the present paper only shows the feasibility of application of ATRP in developing self-healing SIPs, the possible mechanisms involved in the aforesaid embrittlement property are not studied hereinafter.

Conclusion

In summary, ATRP proves to be an effective way to functionalize the surface of GO with polymers. The morphology of the resulting SIPs was studied using TEM and water contact angle studies, while the polymer was characterized by EDX, NMR, GPC, DSC and TGA analysis. EDX and Raman spectroscopy were used to confirm attachment of the initiator to the GO surface in addition to solubility studies. These results indicate that the polymers attached to the GO sheet retained structural features seen in virgin samples of both pristine polymer and GO. Also ATRP is found to be very efficient in providing self-healing ability onto the synthesized polymers. No other chemicals or catalysts are required for healing the cracks except the embedded GMA loaded microcapsules owing to the living polymer matrix. The covalent bonding between the cracked planes established by copolymerization of released GMA and PMMA chains on the surface of GO results in recovery of the strength of the SIPs.

Acknowledgements The authors are grateful to Tezpur University for financial support of this work.

References

1. Guimard NK, Oehlenschlaeger KK, Zhou J, Hilf S, Schmidt FG, Barner-Kowollik C (2012) Current trends in the field of self-healing materials. Macromol Chem Phys 213:131–143
2. Chen X, Dam MA, Ono K, Mal A, Shen H, Nutt SR, Wudl F (2002) A thermally re-mendable cross-linked polymeric material. Science 295:1698–1702
3. Keller MW, White SR, Sottos NR (2007) A self-healing poly (dimethyl siloxane) elastomer. Adv Funct Mater 17:2399–2404
4. Guan Z, Roland JT, Bai JZ, Ma SX, McIntire TM, Nguyen M (2004) Modular domain structure: a biomimetic strategy for advanced polymeric materials. J Am Chem Soc 126:2058–2065
5. Varley RJ, van der Zwaag S (2008) Development of a quasi-static test method to investigate the origin of self-healing in ionomers under ballistic conditions. Polym Test 27:11–19
6. Tadano K, Hirasawa E, Yamamoto H, Yano S (1989) Order-disorder transition of ionic clusters in ionomers. Macromolecules 22:226–233
7. Zare P, Mahrova M, Tojo E, Stojanovic A, Binder WH (2013) Ethylene glycol-based ionic liquids via azide/alkyne click chemistry. J Polym Sci A Polym Chem 51:190–202
8. Gragert M, Schunack M, Binder WH (2011) Azide/alkyne-"click"-reactions of encapsulated reagents: toward self-healing materials. Macromol Rapid Commun 32:419–425

9. Yao L, Yuan YC, Rong MZ, Zhang MQ (2011) Self-healing linear polymers based on RAFT polymerization. Polymer 52:3137–3145
10. Wang HP, Yuan YC, Rong MZ, Zhang MQ (2009) Self-healing of thermoplastics via living polymerization. Macromolecules 43:595–598
11. Kirkby EL, Michaud VJ, Månson JA, Sottos NR, White SR (2009) Performance of self-healing epoxy with microencapsulated healing agent and shape memory alloy wires. Polymer 50:5533–5538
12. Noh HH, Lee JK (2013) Microencapsulation of self-healing agents containing a fluorescent dye. Express Polym Lett 7:88–94
13. Hu J, Chen HQ, Zhang Z (2009) Mechanical properties of melamine formaldehyde microcapsules for self-healing materials. Mater Chem Phys 118:63–70
14. Gao H, Matyjaszewski K (2006) Synthesis of star polymers by a combination of ATRP and the "click" coupling method. Macromolecules 39:4960–4965
15. Ruiz-Muelle AB, Contreras-Cáceres R, Oña-Burgos P, Rodríguez-Dieguez A, López-Romero JM, Fernández I (2018) Polyacrylic acid polymer brushes as substrates for the incorporation of anthraquinone derivatives. Unprecedented application of decorated polymer brushes on organocatalysis. Appl Surf Sci 428:566–578
16. Saikia BJ, Nath BC, Borah C, Dolui SK (2015) Mn2+ anchored CdS polymer nanocomposites: an efficient alternative for Mn2+ doped CdS nanoparticles. J Lumin 168:178–185
17. Yuan YC, Yin T, Rong MZ, Zhang MQ (2008) Self healing in polymers and polymer composites. Concepts, realization and outlook: a review. Express Polym Lett 2:238–250
18. Toomey R, Tirrell M (2008) Functional polymer brushes in aqueous media from self-assembled and surface-initiated polymers. Annu Rev Phys Chem 59:493–517
19. Zhang G, Wu C (2009) Quartz crystal microbalance studies on conformational change of polymer chains at interface. Macromol Rapid Commun 30:328–335
20. Zhou F, Huck WT (2006) Surface grafted polymer brushes as ideal building blocks for "smart" surfaces. Phys Chem Chem Phys 8: 3815–3823
21. Lu Y, Wittemann A, Ballauff M (2009) Supramolecular structures generated by spherical polyelectrolyte brushes and their application in catalysis. Macromol Rapid Commun 30:806–815
22. Matyjaszewski K, Xia J (2001) Atom transfer radical polymerization. Chem Rev 101:2921–2990
23. Percec V, Guliashvili T, Ladislaw JS, Wistrand A, Stjerndahl A, Sienkowska MJ, Sahoo S (2006) Ultrafast synthesis of ultrahigh molar mass polymers by metal-catalyzed living radical polymerization of acrylates, methacrylates, and vinyl chloride mediated by SET at 25 °C. J Am Chem Soc 128:14156–14165
24. Edmondson S, Osborne VL, Huck WT (2004) Polymer brushes via surface-initiated polymerizations. Chem Soc Rev 33:14–22
25. Ding S, Floyd JA, Walters KB (2009) Comparison of surface confined ATRP and SET-LRP syntheses for a series of amino(meth)acrylate polymer brushes on silicon substrates. J Polym Sci A Polym Chem 47:6552–6560
26. Zhu DY, Rong MZ, Zhang MQ (2013) Preparation and characterization of multilayered microcapsule-like microreactor for self-healing polymers. Polymer 54:4227–4236
27. Zhu DY, Wetzel B, Noll A, Rong MZ, Zhang MQ (2013) Thermomolded self-healing thermoplastics containing multilayer microreactors. J Mater Chem A 1:7191–7198
28. Hummers Jr WS, Offeman RE (1958) Preparation of graphitic oxide. J Am Chem Soc 80:1339–1339
29. Bel, T., Ulku, G., Kizilcan, N., Cimenoglu, H., Yahya, N., & Baydogan, N. (2016). Production of microencapsulate glycidyl methacrylate with melamine formaldehyde resin shell materials. In AIP Conference Proceedings (Vol. 1787, No. 1, p. 050028). AIP Publishing
30. Hayes SA, Zhang W, Branthwaite M, Jones FR (2007) Self-healing of damage in fibre-reinforced polymer-matrix composites. J R Soc Interface 4:381–387
31. Jung I, Dikin D, Park S, Cai W, Mielke SL, Ruoff RS (2008) Effect of water vapor on electrical properties of individual reduced graphene oxide sheets. J Phys Chem C 112:20264–20268
32. Savin DA, Pyun J, Patterson GD, Kowalewski T, Matyjaszewski K (2002) Synthesis and characterization of silica-graft-polystyrene hybrid nanoparticles: effect of constraint on the glass-transition temperature of spherical polymer brushes. J Polym Sci B Polym Phys 40:2667–2676
33. Ou B, Li D (2007) Preparation of polystyrene/silica nanocomposites by radical copolymerization of styrene with silica macromonomer. Science in China Series B: Chemistry 50:385–391
34. Wei N, Lv C, Xu Z (2014) Wetting of graphene oxide: a molecular dynamics study. Langmuir 30:3572–3578
35. Badri A, Whittaker MR, Zetterlund PB (2012) Modification of graphene/graphene oxide with polymer brushes using controlled/living radical polymerization. J Polym Sci A Polym Chem 50: 2981–2992
36. Paredes JI, Villar-Rodil S, Martínez-Alonso A, Tascon JMD (2008) Graphene oxide dispersions in organic solvents. Langmuir 24: 10560–10564
37. Shashidhar MS, Bhatt MV (1987) 2-Formylbenzenesulphonyl chloride as a reagent for the protection of phenols. J Chem Soc Chem Commun 9:654–656
38. Brown EN, Kessler MR, Sottos NR, White SR (2003) In situ poly (urea-formaldehyde) microencapsulation of dicyclopentadiene. J Microencapsul 20:719–730
39. Yuan YC, Rong MZ, Zhang MQ (2008) Preparation and characterization of microencapsulated polythiol. Polymer 49:2531–2541
40. Saikia BJ, Dolui SK (2016) Designing semiencapsulation based covalently self-healable poly (methyl methacrylate) composites by atom transfer radical polymerization. J Polym Sci A Polym Chem 54:1842–1851
41. Kim J, Nam DG, Yeum JH, Suh S, Oh W (2015) Characterization of graphite oxide reduced by thermal and/or chemical treatments. Trans Electr Electron Mater 16:274–279
42. Rule JD, Sottos NR, White SR (2007) Effect of microcapsule size on the performance of self-healing polymers. Polymer 48:3520–3529